Chaos in Vallis' asymmetric Lorenz model for *El Niño*

Barnabás M. Garay[a,b,1], Balázs Indig[a]

[a]Faculty of Information Technology, Pázmány Péter Catholic University, Práter utca 50/A, Budapest, Hungary H-1083

[b] Computer and Automation Institute (SZTAKI), Hungarian Academy of Sciences, Kende u. 13–17, Budapest, Hungary H-1111

Email: {garay,indba}@digitus.itk.ppke.hu

Abstract

We consider Vallis' symmetric and asymmetric Lorenz models for *El Niño*—systems of autonomous ordinary differential equations in 3D—with the usual parameters and, in both cases, by using rigorous numerics, locate topological horseshoes in iterates of the respective Poincaré return maps associated to the pair of the "crescent–shaped curves" on a horizontal plane. The minimal number of iterates with the full horseshoe embedded turns out to be two in the symmetric, and three in the asymmetric case, respectively.

Key words: computer–assisted proof for chaos, *El Niño*, shift dynamics

AMS Subject Classification: primary 37N30, secondary 34A26, 37B10, 37N10

[1]Corresponding author.

1 Introduction

The aim of this paper is to give computer–assisted proof for chaos in Vallis' model [25], [26]

$$\dot{x} = By - C(x+p) \quad , \quad \dot{y} = xz - y \quad , \quad \dot{z} = -xy - z + 1 \tag{1}$$

for *El Niño* with parameters $B = 102$, $C = 3$, $p = 0$ in Vallis [25], [26] and $B = 102$, $C = 3$, $p = 0.83$ in Tung [21]. We follow the standard Mischaikow–Mrozek–Zgliczynski approach and look for the full shift on two symbols embedded in some iterates of the Poincaré return map $\Pi = \Pi_p$ associated to the section

$$\mathcal{S} = \{(x, y, z) \in \mathbb{R}^3 \mid z = 0.3 \ \text{ and } \ xy < 0.7\} \, , \tag{2}$$

the subset of a horizontal plane where the vector field points upward. When doing this and restricting our attention to the pairs of the "crescent–shaped curves", an unexpected difference between the symmetric and the asymmetric case is observed. Please compare Figures 2–3 to Figures 4–5 and see Corollary 1 as well.

The general analysis of (1) is parallel to the one of the classical Lorenz system in Sparrow [18]. For $a = a(p) > 0$ sufficiently small and $R = R(p) > 0$ sufficiently large, formula $V(x, y, z) = a(p)x^2 + y^2 + z^2$ defines a quadratic Liapunov function outside the ball of radius R (centered at the origin) and implies that the point at infinity is repulsive. On the other hand, the divergence is $-(C+2)$, a negative constant. Thus, for ($B = 102$, $C = 3$ and) $p \in \mathbb{R}$ arbitrarily given, system (1) admits a compact global attractor $\mathcal{A} = \mathcal{A}_p$ of measure zero.

Both for $p = 0$ and $p = 0.83$, the global attractor $\mathcal{A}_p$ looks like a slightly distorted copy of the standard Lorenz butterfly. (Equilibrium point analysis leads to the same qualitative results.) Actually, for $p = 0$, systems (1) and

$$\dot{x} = \sigma(y - x) \quad , \quad \dot{y} = rx - y - xz \quad , \quad \dot{z} = xy - bz \tag{3}$$

are affinely equivalent [21] — see also Remark 1 below. This is why we feel justified to term (1) as the asymmetric Lorenz model for *El Niño*.

The derivation of Vallis' model is presented in Section 2 below and is followed by a short survey of *El Niño* modelling from the view–point of chaos theory. The main results of the paper are stated in Section 3. Section 4 is

devoted to the computer–assisted proofs themselves. We follow the standard Mischaikow–Mrozek–Zgliczynski approach. (The present paper cannot be considered as a contribution to recent *El Niño* research. Naturally, Vallis [25], [26] himself was fully aware of the unrealistic features of his model.)

2 Between reality and mathematical model

The derivation of system (1) is based on a two–point discretization of the 2D heat advection equation

$$\frac{\partial T}{\partial t} = -\frac{\partial (uT)}{\partial x} - \frac{\partial (wT)}{\partial z} \tag{4}$$

considered in the west–east cross–section of the equatorial Pacific. The cross–section is subdivided by a vertical line and a horizontal line. The vertical line halves the distance between west–east ocean boundaries. The horizontal line is an acceptable substitute for the thermocline separating the warm upper layer of the ocean from the cold water below. Averaged temperatures of the upper ocean layer in the western and eastern Pacific are $T_w = T_w(t)$ and $T_e = T_e(t)$, respectively. Deep ocean temperature under the thermocline is $T_d = \text{const}$. Let U be the velocity of the west–east ocean current at the middle of the upper layer and let W and $-W$ be the velocities of upwelling and downwelling across the thermocline in the middle of the western and eastern ocean basin, respectively. The symmetry between upwelling and downwelling is the result of mass conservation, implying also that $U \cdot \Delta z = W \cdot \Delta x$. Please see the accompanying Figure 1.

Normal velocities are zero at domain boundaries. Hence, centered finite differences give that

$$\dot{T}_w = -\frac{U \cdot \frac{T_w+T_e}{2} - 0}{\Delta x} - \frac{0 - W \cdot \frac{T_w+T_d}{2}}{\Delta z} - \alpha(T_w - T_*) \tag{5}$$

and

$$\dot{T}_e = -\frac{0 - U \cdot \frac{T_w+T_e}{2}}{\Delta x} - \frac{0 - (-W) \cdot \frac{T_e+T_d}{2}}{\Delta z} - \alpha(T_w - T_*) \tag{6}$$

where the correction terms are due to heat exchange with the overlying atmosphere. They express Newtonian damping, with $T_* = \text{const} > T_d$ denoting the temperature to which the ocean would relax in the absence of motion.

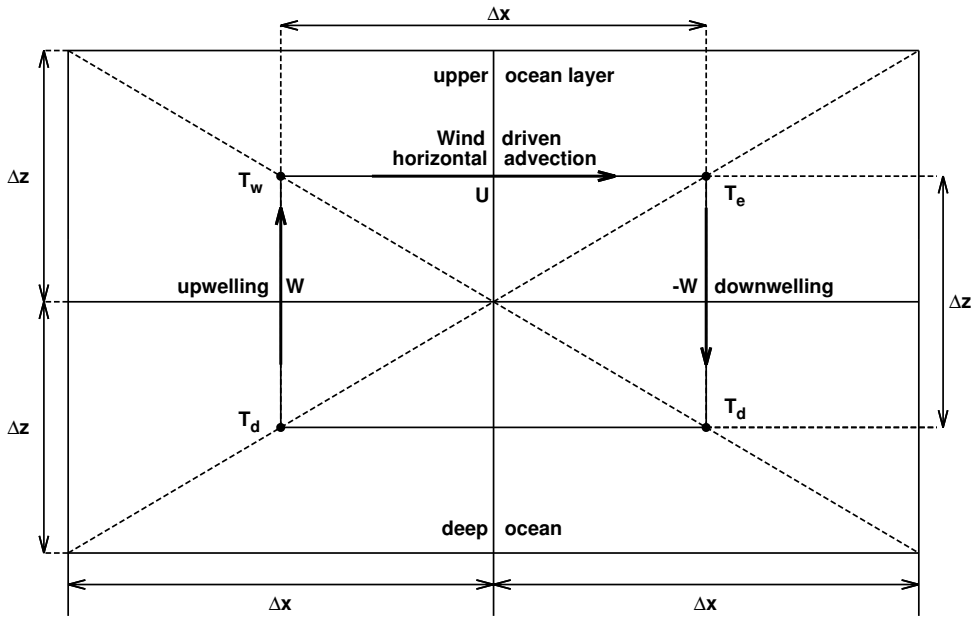

Figure 1: Vallis' model for heat fluctuations in the west–east section of the equatorial Pacific. Here Δx is taken for 7500 kilometers but the value of Δz does not need to be specified. See also Remark 2.

In order to extend (5)–(6) to a closed system, an equation for $U = U(t)$ is needed, too. This equation is

$$\dot{U} = \beta \, \frac{T_e - T_w}{\Delta x} \; - \; \gamma (U - U^*) \, . \tag{7}$$

Here $-\gamma U$ represents mechanical damping, the rest of the right–hand side represents wind produced stress whereas $U^* = \text{const} \leq 0$ stays for the average effect of the trade winds. (The ocean current is driven by the surface wind which, in turn, is generated by the temperature gradient. Variations in pressure are neglected.)

The new variables τ and x, y, z in system (5)–(7) are introduced by letting

$$\tau = \alpha t \quad , \quad x(\tau) = x(\alpha t) \quad , \quad y(\tau) = y(\alpha t) \quad , \quad z(\tau) = z(\alpha t) \, ,$$

$$x(\tau) = \frac{U(t)}{2\alpha \cdot \Delta x} \quad , \quad y(\tau) = \frac{T_e(t) - T_w(t)}{2(T_* - T_d)} \quad , \quad z(\tau) = \frac{T_e(t) + T_w(t) - 2T_d}{2(T_* - T_d)} \, .$$

With τ re–substituted by t at the end of the computation, the standard form of Vallis' asymmetric model (1) is readily obtained.

Remark 1. *Case $p = 0$ of (1) is equivalent to the famous Lorenz system. More precisely, case $p = 0$ of (1) goes over into*

$$\dot{X} = C(Y - X) \quad , \quad \dot{Y} = \frac{B}{C}\, X - Y - XZ \quad , \quad \dot{Z} = XY - Z \tag{8}$$

by the affine coordinate transformation

$$x = -X \quad , \quad y = -\frac{C}{B}\, Y \quad , \quad z = -\frac{C}{B}\, Z + 1\,. \tag{9}$$

With $\sigma = C$, $b = 1$, and $r = \frac{B}{C}$, system (8) is nothing else but (3). In particular, parameters $B = 102$, $C = 3$ correspond to the choice $\sigma = 3$, $b = 1$, $r = 34$.

With great probability, transformation (9) has remained unnoticed for a long time. All we know is that it appears in K.K. Tung's 2007 textbook [21] on mathematical modelling. The 2006 chaos monograph by N.A. Magnitskii and V.A. Sidorov [9] contains a detailed analysis of the bifurcation scenarios of case $p = 0$ of (1) and many similarities to that of the classical Lorenz system are mentioned.

As it is clear from the derivation above, (1) cannot be anything else but a toy model for *El Niño*. This notwithstanding, the parameter triplets $B = 102$, $C = 3$, $p = 0$ in Vallis [25], [26] and $B = 102$, $C = 3$, $p = 0.83$ in Tung [21] carry some physical meaning. Also the chaotic simulation results in [26] and [21] are not absolutely incompatible with *El Niño* observations.

However, existence or non–existence of chaos depends on the grid and the discretization method chosen. As Vallis [26] himself observes, a two–point upwind scheme—when applied to solve the advection equation (4)—results in an apparently bistable 3D system of ordinary differential equations. In fact, considering only the case $U^* = 0$ and $U > 0$, upwind discretization gives that (please see equations (13a)–(14a) in [26])

$$\dot{T}_w = \frac{U}{\Delta x}(T_d - T_w) \; - \; \alpha(T_w - T_*) \quad , \quad \dot{T}_w = \frac{U}{\Delta x}(T_w - T_e) \; - \; \alpha(T_e - T_*)\,.$$

Passing, as before, to the new variables τ and x, y, z, one arrives at the system

$$\dot{x} = By - Cx \quad , \quad \dot{y} = x(-3y + z) - y \quad , \quad \dot{z} = -x(y + z) - z + 1\,. \tag{10}$$

(Equation (7) for U was kept and, as before, τ was re–substituted by t at the end of the computation.) The non–trivial equilibria of system (10) are

$$\mathcal{E}_0^{\pm} = \left(x_0^{\pm}, \frac{C}{B} x_0^{\pm}, \frac{C}{B}(1 + x_0^{\pm}) \right) \qquad \text{where} \quad x_0^{\pm} = \frac{1}{2}\left(-1 \pm \sqrt{\frac{B}{C}} \right) .$$

Thus $x_0^- < 0$ for $B, C > 0$ and $x_0^+ > 0$ if and only if $B > C$. Applying Routh–Hurwitz criterion, a little algebra shows that equilibrium $\mathcal{E}_0^+$, the only equilibrium allowed by condition $U > 0$, is asymptotically stable whenever $B > C > 0$ ([26], with the typing errors corrected).

The situation is the same as with the derivation of the classical Lorenz equations. System (3) is obtained via keeping the first three coefficients in a double Fourier expansion when solving the convection equations of Saltzman. Unfortunately, depending on which Fourier modes are kept, the qualitative properties of the approximating systems of ordinary differential equations differ considerably. Not all of them are chaotic and even if chaotic, the dynamical behaviour at the onset of chaos varies on a case to case basis. This is a widely studied area of research [12], [16]. (Returning to equation (4), it is doubtful if the discrepancies can be resolved by passing to a finer horizontal grid spacing.)

In our present understanding [4], [17], it is very unlikely that *El Niño* phenomena can be adequately modelled by a low–dimensional dynamical system. Remaining in the realm of "simple" approaches, delayed oscillator models based on ocean wave dynamics along the thermocline are considered as more realistic. In what follows τ stays for the time lag between wave generation and arrival in the eastern basin via reflection off the western ocean boundary and $x = x(t)$ can be roughly identified with $T_e = T_e(t)$. In an interesting paper by Redmond, LeBlanc, and Longtin [15], the Suarez–Schopf model [19]

$$\dot{x}(t) = x(t) + \alpha x(t - \tau) - x^3(t) \tag{11}$$

and the Battisti–Hirst model [3]

$$\dot{x}(t) = x(t) + \alpha x(t - \tau) - \beta(x(t) - \gamma x(t - \tau))^3 \tag{12}$$

are presented in a unified framework. Both are considered as truncated Taylor expansions of the general delay–differential system $\dot{x}(t) = f(x(t), x(t-\tau))$

around $(0,0) \in \mathbb{R} \times \mathbb{R}$. Here again, qualitative dynamics depends heavily on the truncation. For all reasonable parameter values, equation (11) admits a compact global attractor. The fine structure of this global attractor is not fully understood. However, the Poincaré–Bendixson type theorem of Mallet–Paret and Sell [10] can be applied to show that chaos is excluded, and that the attractor of slow oscillation is a 2D disc [8]. It is suspected that this 2D disc attracts an open dense subset of the phase space as in [11]. On the other hand, when equipped with the original Battisti–Hirst parameters, equation (12) seems to be chaotic [24]. The claim is supported by strong numerical evidence. The general development of rigorous numerics for infinite–dimensional problems—in particular, recent advances by Lesssard, Mischaikow, Tucker, Zgliczynski and their coworkers—suggests that computer–assisted proofs for topological horseshoes in delay–differential equations will be possible in the near future. Equation (12) with $\beta = 0$ but $\tau = \tau(t,x)$ has been investigated in [5].

Remark 2. *The thermocline depth in the equatorial Pacific is about 200 meters at the western and about 50 metres at the eastern ocean boundary. The El Niño phenomenon is essentially a deepening of the thermocline and an anomalous, Christmas time warming of the coastal waters off Peru and Ecuador about every 3 to 6 years. Thermocline displacements at the eastern boundary can be modelled by*

$$\dot{h}_E(t) = \alpha A_\kappa(h_E(t-\tau)) - \beta A_\kappa(h_E(t-\sigma)) + \gamma \cos(\omega_a t)\,, \qquad (13)$$

a differential–delay equation with two time lags [23]. Here A_κ is a uniformly bounded family of sigmoid functions (parametrized by $\kappa > 0$, the slope at $h_E = 0$) and ω_a is the annual frequency of the idealized seasonal forcing. As κ is increased, equation (13) follows the quasiperiodic route to chaos. The quasiperiodic route to chaos is confirmed and refined in (two slightly different versions of) the Zebiac–Cane model, too [7], [22].

The Zebiac–Cane model plays a central role in the ENSO literature [4], [17]. It is the first model to make *El Niño* prediction possible. The extremely strong 1997/98 *El Niño* episode was successfully forecasted on the basis of the Zebiac–Cane model, a coupled atmosphere–ocean model for the entire tropical Pacific. Note that (12) is a simplification of the Zebiac–Cane model.

In spite of its saintly name, *El Niño* (while referring to the Christ child) has a *"devilishly irregular behaviour"* [7], more complicated than the great

variety of its mathematical models. Both nature and source of this irregularity are only rudimentarily understood. The available time series are too short and the data is not accurate enough. The reader is kindly referred to the *"Noise or chaos? Stable or unstable? Linear or nonlinear? Does it matter and can we tell?"* discussion on pages 280–283 of the monograph of Sarachik and Cane [17].

3 The main results of the present paper

Computer simulation with low resolution suggests that $\mathcal{A}_p \cap \mathcal{S}$ is the union of two crescent–shaped curves. For $p = 0$ and $p = 0.83$, we define the upper and the lower branch of $\mathcal{A}_p \cap \mathcal{S}$ as

$$\mathcal{C}_u^S = \{(x, y, 0.3) \in \mathcal{A}_0 \mid y - 0.207 > \frac{-0.212 - 0.207}{-3.343 - 3.202}(x - 3.202)\} , \quad (14)$$

$$\mathcal{C}_u^A = \{(x, y, 0.3) \in \mathcal{A}_{0.83} \mid y - 0.209 > \frac{-0.199 - 0.209}{-3.531 - 2.855}(x - 2.855)\} , \quad (15)$$

$$\mathcal{C}_\ell^S = \mathcal{A}_0 \cap \mathcal{S} \setminus \mathcal{C}_u^S \quad , \quad \mathcal{C}_\ell^A = \mathcal{A}_{0.83} \cap \mathcal{S} \setminus \mathcal{C}_u^A .$$

From now on, parameter values $p = 0$ and $p = 0.83$ will be referred to by the upper indices S and A (symmetry versus asymmetry), respectively. The upper and the lower branches are compact and disjoint subsets of $\mathcal{S}$ but they are not curves at all. The more zooming in, the more details of a Cantor book structure visible. However, high resolution figures would not help the heuristics we follow.

To the purposes of the present paper, the set $\mathcal{A}_p \cap \mathcal{S}$ is represented by the sequence of consecutive upward intersections between the trajectory starting from the point $P^* = (0.5, 1, 0.3) \in \mathcal{S}$ and the plane of equation $z = 0.3$. More precisely, forgetting about the last coordinate of the k–th upward intersection point

$$\Pi_0^k(P^*) = (x_k^S(P^*), y_k^S(P^*), z_k^S(P^*)) = (x_k^S(P^*), y_k^S(P^*), 0.3) \in \mathcal{S} ,$$

the set $\mathcal{A}_0 \cap \mathcal{S}$ is visualized by the finite sequence

$$(x_k^S(P^*), y_k^S(P^*)) \in \mathbb{R} \times \mathbb{R} , \quad k = 50, 51, \ldots, 100000 .$$

For Lorenz system (3) with the classical parameters, a celebrated result of Tucker [20] states that such an identification—in the well-defined technical sense of robustness and SRB measures—is fully justified.

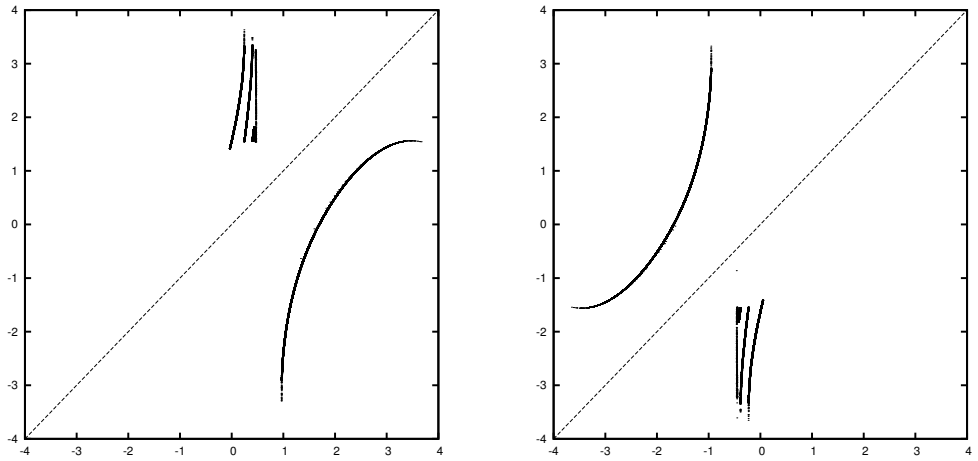

Figure 2: The graphs of the Lorenz type maps $M^S_{u,1}$ (left panel) and $M^S_{\ell,1}$ (right panel)

For $n = 1, 2, 3$ (there is no need of going any further), a quadruple of Lorenz type maps

$$M^I_{i,n} : x^I_k(P^*) \to x^I_{k+n}(P^*) \ , \quad I = S, A \quad \text{and} \quad i = u, \ell$$

is introduced, simply by specifying the respective domains. For $I = S, A$ and $i = u, \ell$, the domain of $M^I_{i,n}$, $n = 1, 2, 3$ is chosen for the subsequence with indices $50 \le k \le 100000 - n$ such that

$$(x^I_k(P^*), y^I_k(P^*), 0.3) \in \mathcal{C}^I_i \quad \text{and} \quad (x^I_{k+n}(P^*), y^I_{k+n}(P^*), 0.3) \in \mathcal{C}^I_i \ .$$

Though its domain consists of only a finite set of points, we consider $M^I_{i,n}$ as if it were defined and continuous on a finite union of open intervals. This heuristics is made possible by an optical illusion due to the relative denseness of the actual domains. The graphs of mappings $M^S_{u,1}$ & $M^S_{\ell,1}$, $M^S_{u,2}$, $M^A_{u,2}$ & $M^A_{\ell,2}$ and $M^A_{u,3}$ are shown in Figures 2, 3, 4 and 5, respectively. Observe the tremendous difference between Figures 3 and 4. This comes as a surprise because $\mathcal{C}^A_u$ and $\mathcal{C}^S_u$ are pretty much the same (whereas $\mathcal{C}^A_\ell$ is about 15% "shorter" than $\mathcal{C}^S_\ell$).

Now we are in a position to state our finding.

Corollary 1. *Consider equation (1) with parameters $B = 102$, $C = 3$ and recall that Π^n_p denotes the n–th iterate of the Poincaré return map associated to section (2).*

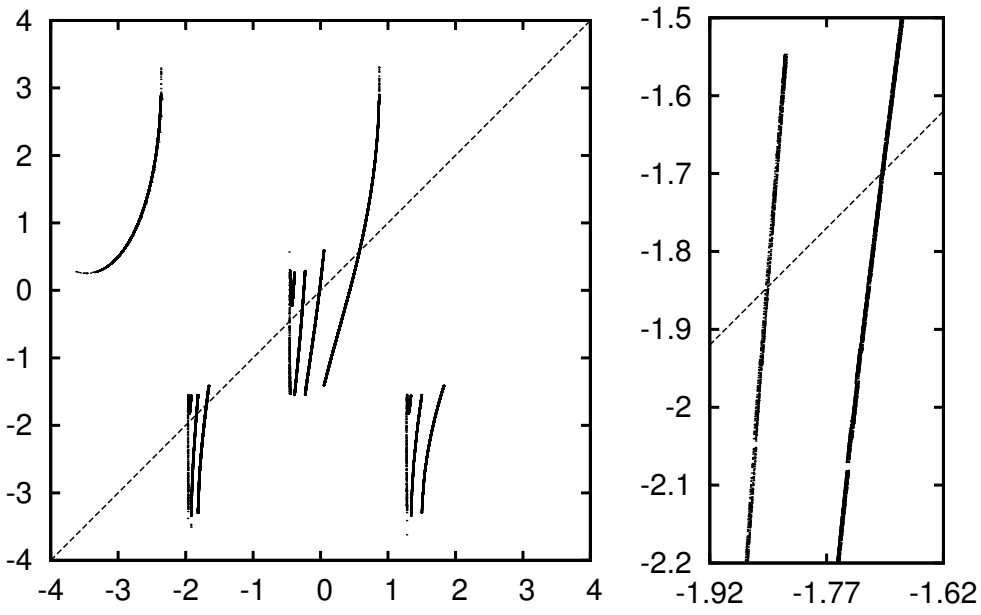

Figure 3: The graph of $M^S_{u,2}$, with a magnified and rescaled view of a selected area (for determining the values of δ, γ, β and α)

For $p = 0$, Π_p^2 admits a Σ_2–chaos on $\mathcal{C}_u^S$ defined in (14). The result does not hold true for Π_p itself, neither on $\mathcal{C}_u^S$ nor on $\mathcal{C}_\ell^S$.

For $p = 0.83$, Π_p^3 admits a Σ_2–chaos on $\mathcal{C}_u^A$ defined in (15). The result does not hold true for Π_p and Π_p^2 themselves, neither on $\mathcal{C}_u^A$ nor on $\mathcal{C}_\ell^A$.

The strategy is to see if elementary chaos results in one dimension apply for $M^I_{i,1}$, i.e., for what looks like the graph of the underlying real function ($I = S, A$ and $i = u, \ell$). If not, we pass from $M^I_{i,1}$ to $M^I_{i,2}$ etc. The two intervals obtained in this manner will serve as an educated initial guess in choosing the critical quadrangles needed for a successful application of Theorem 1, the core of most computer–assisted proofs for topological horseshoes in two dimension.

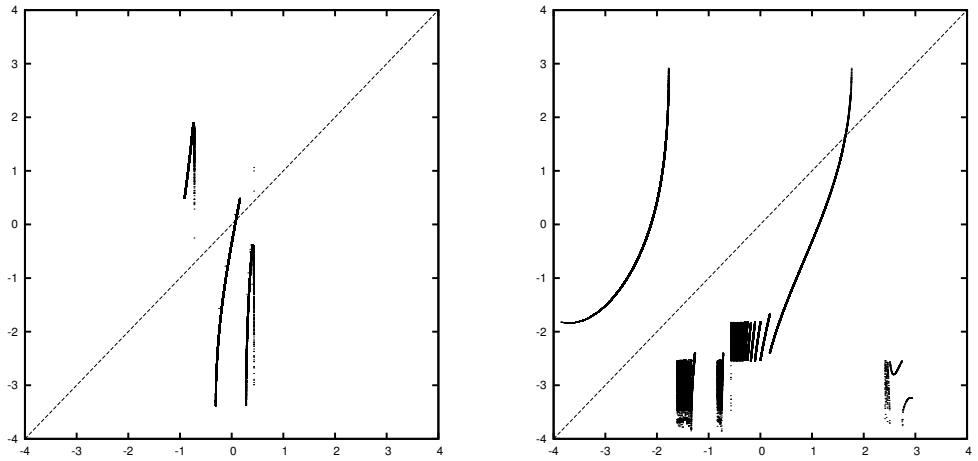

Figure 4: The graphs of the Lorenz type maps $M^A_{u,2}$ (left panel) and $M^A_{\ell,2}$ (right panel)

4 The proof of Corollary 1

The following theorem is a slight reformulation of the main result in Zgliczynski [27]. A simple proof (working also in the higher–dimensional setting [2]) is given in [1].

Theorem 1. *Set* $X = \mathbf{R}^2$. *With* $x = (x_1, x_2) \in \mathbf{R} \times \mathbf{R} = X$, *define*

$$E = \left\{ x \in X \;\middle|\; 1 \le |x_1| \le 2\,,\ |x_2| \ge 2 \right\}\ ,\ O_C = \{ x \in X \;\big|\; |x_1| < 1 \}\,,$$

$$R = \{ x \in X \;\big|\; 1 \le x_1 \le 2, |x_2| \le 2 \}\ ,\ O_R = \{ x \in X \;\big|\; x_1 > 2 \}\,,$$

$$L = \{ x \in X \;\big|\; -2 \le x_1 \le -1, |x_2| \le 2 \}\ ,\ O_L = \{ x \in X \;\big|\; x_1 < -2 \}\,,$$

$$a = R \cap cl(O_R)\,,\ b = R \cap cl(O_C)\,,\ c = L \cap cl(O_C)\,,\ d = L \cap cl(O_L)\,.$$

Consider a homeomorphism φ *of* $L \cup R$ *onto* $\varphi(L \cup R)$ *and suppose that*

$$\varphi(a) \cup \varphi(c) \subset O_R\ ,\ \varphi(b) \cup \varphi(d) \subset O_L\ ,\ \ \textit{and}\ \ \varphi(L \cup R) \subset X \setminus E\,. \tag{16}$$

Then mapping

$$\sigma : \Lambda_\varphi = cl(\{\varphi\textit{–periodic points with trajectories in}\ \ L \cup R\}) \to \Sigma_2$$

defined by

$$(\sigma(x))_k = \begin{cases} 0 & \textit{whenever}\ \ \varphi^k(x) \in L \\ 1 & \textit{whenever}\ \ \varphi^k(x) \in R \end{cases} \qquad \textit{for each}\ \ x \in \Lambda_\varphi\,,\ k \in \mathbb{Z}$$

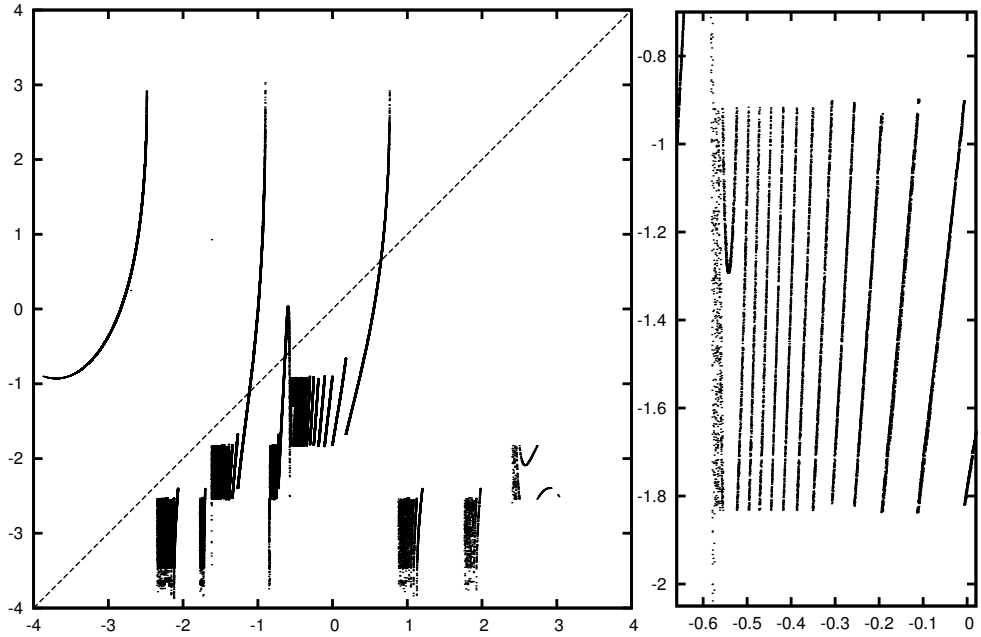

Figure 5: The graph of $M^A_{u,3}$, with a magnified and rescaled view of a selected area (just for fun; the values of $\delta \approx -1.2$, $\gamma \approx -0.97$, $\beta \approx 0.25$ and $\alpha \approx 0.7$) can be read from the left panel of the figure

is continuous, onto and satisfies $\sigma\varphi = S\sigma$ *on* Λ_φ. *In particular,* $\varphi|_{\Lambda_\varphi} : \Lambda_\varphi \to \Lambda_\varphi$ *is semiconjugate to* $\sigma : \Sigma_2 \to \Sigma_2$, *the left shift operator on the space of doubly infinite* 0–1 *sequences (equipped with the product topology).*

In most applications, including those below, the set–up is homeomorphic to the horizontal–vertical set–up of Theorem 1 whereas L and R are chosen for quadrangles. See Figure 6.

Now we are ready to prove the first part of the Corollary. Inspecting the right panel of Figure 3, our first choice for L and R are

$$L_{init} = \mathrm{conv}\{\{\delta\} \times [M^S_{u,2}(\delta) - \varepsilon, M^S_{u,2}(\delta) + \varepsilon]\,,\, \{\gamma\} \times [M^S_{u,2}(\gamma) - \varepsilon, M^S_{u,2}(\gamma) + \varepsilon]\,\}$$

and

$$R_{init} = \mathrm{conv}\{\{\beta\} \times [M^S_{u,2}(\beta) - \varepsilon, M^S_{u,2}(\beta) + \varepsilon], \{\alpha\} \times [M^S_{u,2}(\alpha) - \varepsilon, M^S_{u,2}(\alpha) + \varepsilon]\},$$

respectively. Here $\delta \approx -1.86$, $\gamma \approx -1.82$, $\beta \approx -1.73$, $\alpha \approx -1.68$ with $\delta, \gamma, \beta, \alpha$ belonging to the domain of $M^S_{u,2}$ and constant $0 < \varepsilon \ll 1$ has still to

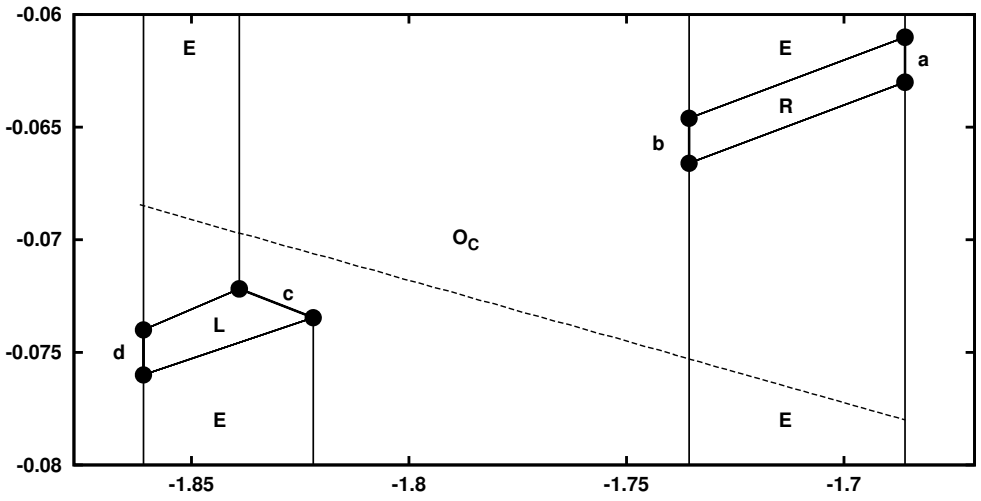

Figure 6: The critical quadrangles in proving the first part of Corollary 1. The almost straight dashed line between L and R shows a portion of $\mathcal{S} \cap \mathcal{M}^s(0,0,1)$, the intersection between $\mathcal{S}$ and the stable manifold of equilibrium $(0,0,1) \in \mathbb{R}^3$.

be specified. The idea is if we had a continuous function $M : [\delta, \gamma] \cup [\beta, \alpha] \to \mathbb{R}$ with the properties that

$$M([\delta, \gamma]) \supset [\delta, \gamma] \cup [\beta, \alpha] \quad , \quad M([\beta, \alpha]) \supset [\delta, \gamma] \cup [\beta, \alpha]$$

(a Li–Yorke sufficient condition for chaos in one dimension) and that both $M|_{[\delta,\gamma]}$ and $M|_{[\beta,\alpha]}$ are strictly increasing.

From a purely theoretical view–point, the problem of finding the appropriate quadrangles that satisfy condition (16) is a constraint satisfaction problem in rigorous global optimization. Requiring that the eight half–lines (determining the taboo set E) are all vertical, one has to work with 16 parameters, the coordinates of two general rectangles L and R. With $\varepsilon = 0.01$, parallelograms L_{init} and R_{init} can serve as initial data for this procedure. Though the method works for iterates of the classical Hénon mapping [1], its combination with a rigorous ODE solver seems to be too involved for us. We follow the pedestrian approach instead and refine L_{init} and R_{init} by nonrigorous and nonautomatic methods. Also the choice for the horizontal plane $z = 0.3$ is the result of an earlier computer experimentation.

As for the first part of Corollary 1, we set

$$\varphi = \Pi_0^2 \quad , \quad L = \mathrm{conv}\{\mathbf{d}, \mathbf{c}\} \quad , \quad R = \mathrm{conv}\{\mathbf{b}, \mathbf{a}\} \tag{17}$$

with the straight line segments $\mathbf{d}, \mathbf{c}, \mathbf{b}, \mathbf{a} \subset \mathcal{S}$ chosen for

$$\begin{aligned}
\mathbf{a} &= \mathrm{conv}\{(-1.686, -0.061, 0.3), (-1.686, -0.063, 0.3)\} , \\
\mathbf{b} &= \mathrm{conv}\{(-1.7356, -0.0646, 0.3), (-1.7356, -0.0666, 0.3)\} , \\
\mathbf{c} &= \mathrm{conv}\{(-1.839, -0.07218, 0.3), (-1.822, -0.07346, 0.3)\} , \\
\mathbf{d} &= \mathrm{conv}\{(-1.861, -0.074, 0.3), (-1.861, -0.076, 0.3)\} .
\end{aligned}$$

See Figure 6 again.

As for the second part of Corollary 1, we set

$$\varphi = \Pi_{0.83}^3 \quad , \quad L = \mathrm{conv}\{\mathbf{d}, \mathbf{c}\} \quad , \quad R = \mathrm{conv}\{\mathbf{b}, \mathbf{a}\} \tag{18}$$

with the straight line segments $\mathbf{d}, \mathbf{c}, \mathbf{b}, \mathbf{a} \subset \mathcal{S}$ chosen for

$$\begin{aligned}
\mathbf{a} &= \mathrm{conv}\{(0.66, 0.133, 0.3), (0.66, 0.1357, 0.3)\} , \\
\mathbf{b} &= \mathrm{conv}\{(0.24, 0.1093, 0.3), (0.24, 0.112, 0.3)\} , \\
\mathbf{c} &= \mathrm{conv}\{(-0.95, 0.0314, 0.3), (-0.95, 0.0335, 0.3)\} , \\
\mathbf{d} &= \mathrm{conv}\{(-1.18, 0.0144, 0.3), (-1.18, 0.0165, 0.3)\} .
\end{aligned}$$

The rigorous ODE solver we use is the VNODE package developed by Ned Nedialkov [14]. We work with the most current, Literate Programming C++ version. Given an initial value problem, the solver computes an interval enclosures of the exact solution at various time instance, including the endpoint of a prescribed time interval. Now suppose that the initial value belongs to a Poincaré section of an autonomous ordinary differential equation. When combined with an adaptive time subdivision algorithm, VNODE can be used to compute two interval enclosures of the exact solution, belonging to time instants slightly less and slightly greater than the return time, respectively. Geometrically, we arrive at tiny boxes on opposite sides of the Poincaré section. Lowering the tolerance, the size of these boxes can be made smaller and smaller. By means of Gronwall inequality, we end up with a tiny, codimension one interval enclosure of the intersection point between the exact trajectory and the Poincaré section, an interval which is a subset of the Poincaré section. In our special case of equation (1), we arrive at a tiny rectangle on the plane of equation $z = 0.3$ in $\mathbb{R}^3$.

In order to check if condition (16) is satisfied, VNODE has to be combined with an adaptive branch and bound space subdivision algorithm as well. In our special case, the space to be subdivided is two–dimensional.

For both data sets (17) and (18), condition (16) was checked on an eight core 3.4GHz computer. The total CPU time was slightly longer than two days.

The program we used can be downloaded at https://github.com/dlazesz/chaos

The negative statements in Corollary 1 follow via the lack of fixed points for Π_0 on $\mathcal{C}_u^S$ and on $\mathcal{C}_\ell^S$ and via the uniqueness of fixed points for $\Pi_{0.83}^2$ on $\mathcal{C}_u^A$ and on $\mathcal{C}_\ell^A$, respectively.

Quadrangles chosen by Mischaikow and Mrozek [13] and by Galias and Zgliczynsky [6] to locate topological horseshoes in the dynamics of the Lorenz system—actually, in the dynamics of the second iterate of the respective Poincaré return maps—were parallelograms. Using the notation of the present paper (in a somewhat loosely way), all those parallelograms had a nonempty intersection with $\mathcal{C}_u^S$ and with $\mathcal{C}_\ell^S$. Please see Figure 1 in [13] and Figure 3 in [6].

References

[1] B. Bánhelyi, T. Csendes and B.M. Garay, Optimization and the Miranda approach in detecting horseshoe–type chaos by computer, *Int. J. Bifurc. Chaos* **17**(2007), 735–748.

[2] B. Bánhelyi, T. Csendes, B.M. Garay and L. Hatvani, A computer-assisted proof for Σ_3–chaos in the forced damped pendulum equation, *SIAM J. Appl. Dyn. Syst.* **7**(2008), 843–867.

[3] D.S. Battisti and A.C. Hirst, Interannual variability in a tropical atmosphere-ocean model: influence of the basic state, ocean geometry and nonlinearity, *J. Atmos. Sci.* **46**(1989), 1687–1712.

[4] A.J. Clarke, *An Introduction to the Dynamics of El Nino and the Southern Oscillation*, Elsevier, Amsterdam, 2008.

[5] A.J. Clarke, J. Wang and S. Van Gorder, A simple warm–pool displacement ENSO model, *J. Phys. Oceanogr.* **30**(2000), 1679-1691.

[6] Z. Galias and P. Zgliczynski, Computer assisted proof of chaos in the Lorenz system, *Physica D*, **115**(1998), 165–188.

[7] F.F. Jin, J.D. Neelin and M. Ghil, *El Niño* on the devil's staircase: Annual subharmonic steps to chaos, *Science*, **264**(1994), 70–72.

[8] T. Krisztin, The global attractor of slow oscillation for monotone negative feedback with time delay (in preparation)

[9] N.A. Magnitskii and S.V. Sidorov, *New Methods for Chaotic Dynamics*, World Scientific, Singapore, 2006.

[10] J. Mallet–Paret and G. Sell, The Poincaré–Bendixson theorem for monotone cyclic feedback systems with delay, *J. Diff. Eq.* **125**(1996), 441-489.

[11] J. Mallet–Paret and H.-O. Walther, Rapid oscillations are rare in scalar systems governed by monotone negative feedback with a time delay, Preprint, Math. Inst., University of Giessen, 1994.

[12] P.S. Marcus, Effects of truncation in modal representations of thermal convection, *J. Fluid Mech.*, **103**(1981), 241-255.

[13] K. Mischaikow and M. Mrozek, Chaos in the Lorenz equations: a computer assisted proof. Part II: Details, *Math. Comp.* **67**(1998), 1023–1046.

[14] N.S. Nedialkov, Implementing a Rigorous ODE Solver through Literate Programming, Technical Report, McMaster University, 2010.

[15] B.F. Redmond, V.G. LeBlanc and A. Longtin, Bifurcation analysis of a class of first–order nonlinear delay–differential equations with reflectional symmetry *Physica D* **166**(2002), 131-146.

[16] D. Roy and Z.E. Musielak, Generalized Lorenz models and their routes to chaos. I. Energy-conserving vertical mode truncations. *Chaos Solitons & Fractals*, **32**(2007), 1038–1052.

[17] E.S. Sarachik and A.M. Cane, *The El Niño–Southern Oscillation Phenomenon*, Cambridge University Press, Cambridge, 2010.

[18] C. Sparrow, *The Lorenz Equations: Bifurcations, Chaos, and Strange Attractors*, Springer, Berlin, 1982.

[19] M.J. Suarez and P.S. Schopf, A delayed action oscillator for ENSO, *J. Atmos. Sci.* **45**(1988), 3283–3287.

[20] W. Tucker, A rigorous ODE solver and Smale's 14th problem", *Found. Comp. Math.* **2**(2002), 53-117.

[21] K.K. Tung, *Topics in Mathematical Modeling*, Princeton University Press, Princeton, R.I., 2007.

[22] E. Tziperman, M.A. Cane and S.E. Zebiak, Irregularity and locking to the seasonal cycle in an ENSO prediction model as explained by the quasi–periodicity route to chaos, *J. Atmos. Sci.* **55**(1995), 293–306.

[23] E. Tziperman, L. Stone, A.M. Cane and H. Jarosh, *El Niño* chaos: Overlapping of resonances between the seasonal cycle and the Pacific ocean–atmosphere oscillator, *Science*, **264**(1994), 72–74.

[24] M. Umeki, Chaos in the Battisti–Hirst original model for El Nino Southern Oscillation, *Theor. Appl. Mech. Japan* **60**(2012), 21–27.

[25] G.K. Vallis, *El Niño* — a chaotic dynamical system? *Science*, **232**(1986), 243–245.

[26] G.K. Vallis, Conceptual models of *El Niño*/Southern Oscillation, *J. Geophys. Res.*, **93**(1988), 13979–13991.

[27] P. Zgliczynski, Fixed point index for iterations of maps, topological horseshoe and chaos, *Topol. Methods Nonlin. Anal.* **8**(1996), 169–177.